Indian Journal of Pure & Applied Physics
Vol. 64, July 2026, pp. 737-745
DOI: 10.56042/ijpap.v64i7.29641

Frequency Stabilization of Renewable Energy Sources and Redox Flow Battery Integrated Three Area Power System Using Cascade Controller

Ram Ishwar Vais[a], Vijay Pal Singh[b], Mratyunjay Singh[c], Ashish Tripathi[c], Sarvesh Kumar[c*] & Tirumalasetty Chiranjeevi[d]

[a]Department of Electrical Engineering, Rajkiya Engineering College, Sonbhadra 231 206, India
[b]Department of Electrical Engineering, Rajkiya Engineering College, Bijnor 246 725, India
[c]Department of Electrical Engineering, Rajkiya Engineering College, Banda 210 201, India
[d]School of Electrical Engineering, Shri Mata Vaishno Devi University, Katra 182 320, India

Received: 11th March 2026; accepted: 5th May 2026

This paper proposes a novel cascaded PID–TID (proportional–integral–derivative and tilt–integral–derivative) control strategy for a three-area interconnected power system integrating a thermal system (TS), wind turbine system (WTS), electric vehicles (EVs), and a redox flow battery (RFB) as an energy storage device (ESD). A comprehensive MATLAB/Simulink model of the system is developed to evaluate dynamic performance under varying operating conditions. The controller parameters are optimally tuned using the Mayfly Optimization Algorithm (MOA) to ensure superior control action. The effectiveness of the proposed cascaded PID–TID controller is validated through comparative analysis with conventional standalone PID and TID controllers. Simulation results demonstrate that the proposed approach significantly enhances oscillation damping, reduces settling time, and minimizes peak overshoot and undershoot. In addition, the impacts of WTS, EVs, and ESD integration on system dynamics are systematically investigated, showing notable improvements in frequency regulation and transient stability. Sensitivity analysis further confirms the robustness and reliability of the proposed control scheme, indicating its suitability for modern multi-area power systems with high penetration of renewable energy sources.

Keywords: Automatic generation control, Cascade controllers, Energy storage device, Electric vehicle, Wind turbine system

1 Introduction

Modern power systems are becoming increasingly complex due to their continuous expansion. As a result, it is now more difficult to maintain an appropriate generation-load balance while keeping the system frequency within reasonable limit. Automatic Generation Control (AGC) is crucial for addressing these challenges. Its core objectives are to design a reliable control strategy, ensure frequency stability, and maintain equilibrium between power generation and demand[1,2]. While early AGC research primarily targeted single-area thermal systems (TSs), current studies increasingly focus on multi-area, multi-source power systems[3]. The AGC research continues to evolve, with an expanding and increasingly complicated variety of elements requiring attention during analysis and implementation. Using renewable energy sources (RES) like wind turbine systems (WTS) and solar thermal power plants into AGC frameworks has been the subject of relatively few studies[4,5]. AGC models containing WTS have been examined under the simplifying assumption of constant wind speed[6–8]. However, it is crucial to remember that because wind is intermittent, WTS's real power output is always changing.

With distributed energy storage, the quick development of electric vehicle (EV) technology is expected to be essential for guaranteeing emergency reliability services. Furthermore, the environmental advantages of EVs, such as their ability to reduce carbon dioxide emissions and reliance on fossil fuels, are contributing to their growing popularity. The suitability of EV technology for low inertia power networks has been investigated[9,10]. These studies indicate that incorporating EVs into multi-area power systems offers considerable scope for advancement and therefore requires more comprehensive exploration.

The role of ESDs in AGC has been extensively investigated, demonstrating their effectiveness in enhancing system dynamics[11-14]. These studies considered a range of storage technologies, including flywheels, ultra-capacitors, super-capacitors, battery energy storage systems, and redox flow batteries (RFBs). Furthermore, the application of energy storage systems to hybrid power systems incorporating multiple renewable energy sources and

*Corresponding author: E-mail: tricalsarvesh@gmail.com

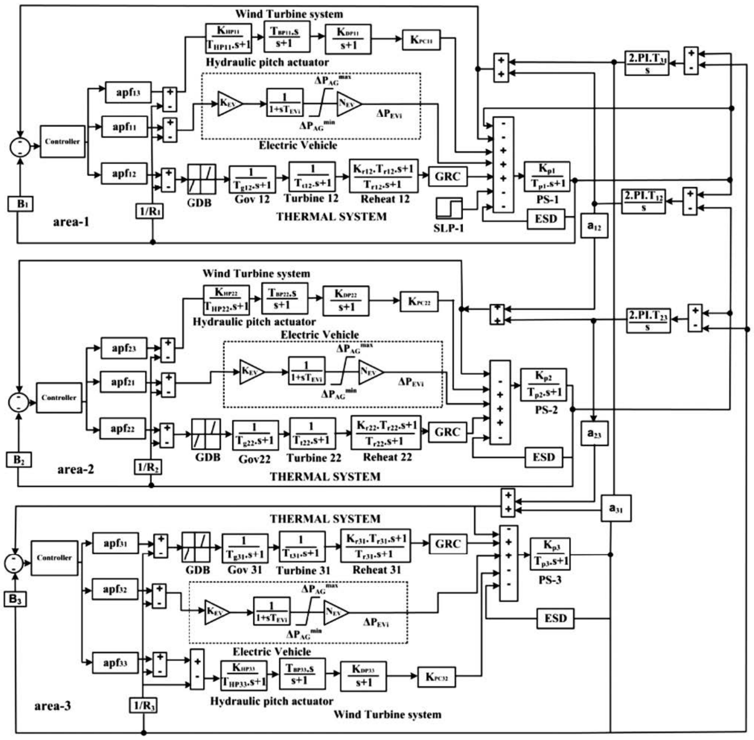

Fig. 1 — Proposed Simulink model

electric vehicles has been investigated[15]. The reported results indicate that RFBs outperform other energy storage technologies in terms of dynamic performance and stability improvement.

Research on AGC has predominantly emphasized the scheme of secondary controllers, leading to the development of various structures such as fractional-order, cascade, and integer-order controllers. Notable examples include the Tilt–Integral–Derivative (TID) controller[16,17] and simpler fractional-order (FO) forms like I, PI, and PID controllers[18]. Further various types of cascade controller like, PI-PD[19], FOPI- FODF[20], PI-FOPID[18,21] etc. Though these developments have been made, a thorough comparison study is still required to assess how well these controllers work in multi-area AGC systems that are connected to EVs and ESD. Therefore, this study proposes a novel PID-TID controller to address this research gap and enhance AGC performance under such operating conditions.

Recent research in AGC has shown a clear trend toward employing metaheuristic optimization techniques for tuning controller parameters. Representative approaches include Cuckoo Search[22], Butterfly Optimization[18], Tunicate Swarm Algorithm[23], Bird Swarm Algorithm[24], Emperor Penguin Algorithm[25], Artificial Rabbit Optimization[26], and Crow Search Algorithm[27,28]. Among these, the Mayfly Optimization Algorithm (MOA), inspired by the flight patterns and reproductive behaviour of mayflies, integrates features of both evolutionary computation and swarm intelligence[29]. While MOA has demonstrated effectiveness in several domains, its application to AGC remains unexplored, highlighting the need for a comprehensive investigation into its suitability for optimizing controller parameters in this context.

2 Materials and Methods

2.1 System Under Investigation

Figure 1 shows the Simulink model of a three-unequal-area TS consisting of WTS, EVs and RFB as ESD. The nominal parameters of the TS, adopted from[8,20], are provided in the Appendix. Several secondary controllers, including TID, PID, and the cascaded PID–TID, are considered for evaluation, and the corresponding dynamics are analyzed in detail. The newly developed MOA, a metaheuristic optimization method, is used for optimization. The Integral Squared Error (ISE) in (1) is used as the optimization process to minimize the performance metric. The system deviations that occur from applying a 1 % step load perturbance (SLP) in area-1 are measured to evaluate the system dynamics.

$$J_{\text{ISE}} = \int_0^t \{(\Delta \text{F}_m)^2 + (\Delta \text{P}_{\text{m-n}})^2\}.\text{dt} \quad \ldots (1)$$

2.2 System Components

The system investigated in Fig.1 comprises TS, WTS, EV and RFB and are explained below

2.2.1 Modelling of Thermal System

The thermal generating unit is modelled to investigate the power plant reaction to changes in frequency and load. The governor with a GDB of ± 0.06 % is considered with reheat turbine and GRC of ± 3 %. The governor dead band is a narrow region of frequency change when mechanical constraints prevent the governor from responding. To control the turbine input and preserve the equilibrium between generation and load, the governor senses variations in frequency and modifies the steam value position.

The generator is provided by the turbine, particularly the reheat turbine which transforms steam energy to mechanical energy. Steam expands gradually in a rehear system as it reheats between turbine sections to increase efficiency. The mathematical equations of governor, turbine and reheat with gains (K) and time constant (T) are in Eqs. (2) – (4).

$$TF_{Governor} = \frac{1}{Tg_i s+1} \quad \ldots (2)$$

$$TF_{Turbine} = \frac{1}{Tt_i s+1} \quad \ldots (3)$$

$$TF_{Re\ heat} = \frac{K_{ri}T_{ri}s+1}{Tr_i s+1} \quad \ldots (4)$$

2.2.2 Modelling of Electric Vehicle

The EV model with ESD is powered by batteries. However, considering the nature of EVs as loads and the flexibility of the system, it results in vibrations in regulation capacity[10]. This introduces a significant amount of uncertainty. Due to the limited power output of a single EV, it cannot independently support frequency control. Therefore, an EV aggregator is necessary for each region to be integrated into the AGC system. These aggregators utilize internal algorithms to receive reports from AGC signals and then distribute them to individual electric vehicles. Essentially, each aggregator contributes to AGC by discharging EV batteries to meet the demand from the grid. Figure 2 provides an illustration of the TF model

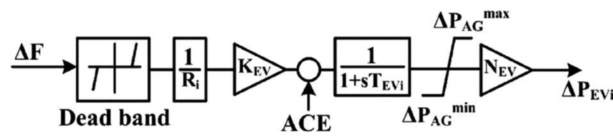

Fig. 2 — TF model of EV aggregator

of the electric vehicle aggregator[30] with gain (K_{EV}) and time constant (T_{EV}). Equations (5) and (6) may be used to calculate the values of ΔPAG_{max} and ΔPAG_{min}.

$$\Delta \text{P}_{\text{AG}}^{\text{max}} = + \left[\frac{1}{N_{\text{EV}}} \times (\Delta \text{P}_{\text{EVi}})\right] \quad \ldots (5)$$

$$\Delta \text{P}_{\text{AG}}^{\text{max}} = - \left[\frac{1}{N_{\text{EV}}} \times (\Delta \text{P}_{\text{EVi}})\right] \quad \ldots (6)$$

where, N_{EV} total no. of EV, the power through each EV's is ΔP_{EVi} .

2.2.3 Modelling of WTS

To support frequency management in power systems using RES, WTS are being incorporated into AGC research. Using turbine blades, a shaft and a generator, wind turbines transform the kinetic energy of wind to electricity. Simplified dynamic models that explain the link between wind speed and generated power suing in AGC models to depict WTS. Wind turbine power output varies and may affect system frequency since wind energy is erratic and unpredictable. To enhance the stability and dependability of contemporary power systems, WTS are coordinated with conventional generators and ESD.

2.2.4 Modelling of RFB

To enable frequency management and enhance system stability, AGC used the RFB device. It can swiftly provide or absorb power during load changes and stores energy in liquid electrolytes with redox active ions. The RFB enhances the performance using RES and helps lower frequency deviation because of tis quick response and adaptable functioning. A simplified dynamic model with gain (k), time constant (T) and state of charge is typically used to describe the RFB in AGC investigations and are in Eq. (7).

$$T_{RFB}(s) = \frac{K_{RFB}}{1+T_{RFB}\,s}\Delta f(s) \quad \ldots (7)$$

2.3 Proposed Cascaded PID-TID Controller

When two or more controllers are cascaded together, the performance of the control system is improved. This technique is often used for the purpose of the quick rejection of disturbances. Since it contains two consecutive processes that increase its dynamic performance, cascading provides several benefits that are not available with a single-loop system. The main loop acts as the master controller, accountable for overseeing the final output of the system. On the other hand, the secondary or inner loop is the slave, and its purpose is to reduce the adverse effects of internal processes. The simple cascade combination with two control loops is shown in Fig. 3. $G_1(s)$ and $G_2(s)$ are the outer and inner processes, respectively. The whole system is subjected to disturbance $d_1(s)$ and produces the output Y(s). The outer loop equations are given by Eq. (8).

$$Y(s) = G_1(s).U_1(s) + d_1(s) \quad \dots (8)$$

From Fig. 3, the input to the outer loop (U1(s)) is an output of the inner loop (ie, $U_1(s) = y_2(s)$). The outer loop $G_1(s)$ should be controlled by a reference signal R(s). The output of the inner loop with inner process unit $U_2(s)$ is given by Eqs. (9) and (10).

$$y_2(s) = G_2(s).U_2(s) \quad \dots (9)$$

$$Y_j(s) = \left(\frac{G_1(s)G_2(s)C_1(s)C_2(s)}{1+G_2(s)C_2(s)+G_1(s)G_2(s)C_1(s)C_2(s)}\right)R_j(s) + \left(\frac{G_1(s)}{1+G_2(s)C_2(s)+G_1(s)G_2(s)C_1(s)C_2(s)}\right)d_j(s) \quad \dots (10)$$

The input for the cascaded controller is the ACE signal, i.e., combinations of frequency and tie-power. Recently, a novel FO controller, termed the Tilt Controller, has been proposed in[20]. Using this controller, it integrates the benefits of both IO-FO into a unified control structure. Taking into consideration these advantages, a novel controller that is referred to as PID-TID is presented in this work. Representations of the structures that make up the proposed controller are provided in Fig. 4.

where, (U(s)) is controller input; K_{Tj} (Tilt gain), K_{Ij} (Integral gain), K_{Dj} (derivative gain). Optimization is run considering the constraints in Eq. (11).

$$0 \le K_{\mathrm{Ti}} \le 1, 0 \le K_{Pi} \le 1,$$
$$0 \le K_{\mathrm{Ii}} \le 1, 0 \le K_{\mathrm{Di}} \le 1,$$
$$2 \le n_i \le 7 \quad \dots (11)$$

Mayfly Optimization Algorithm (MOA)

The MOA, a metaheuristic method based on mayfly mating behaviour, was proposed by[29]. MOA simulates the short lifespan and reproductive behaviour of mayflies and is designed to effectively tackle complicated optimization issues. The method starts by creating a population of candidate solutions, each of whom stands for a possible fix for the issue. The algorithm refines the solution set across future generations by reproducing the adaptive modifications and enhancements seen in wild mayfly mating behaviour through iterative updates. The population is split into two categories by the algorithm with each

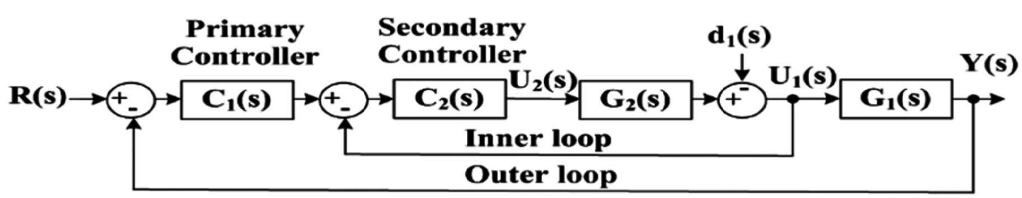

Fig. 3 — Bock diagram of cascade control

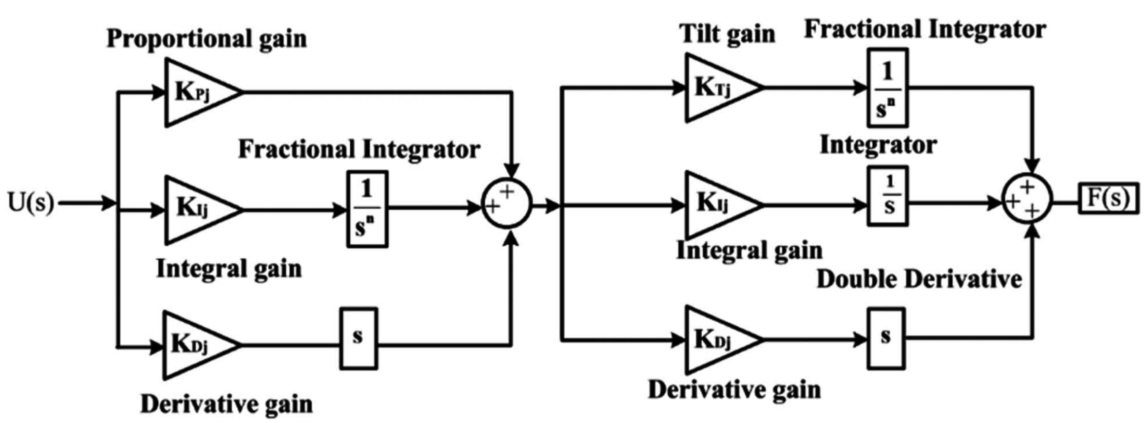

Fig. 4 — Cascaded PID- TID controller

Table 1 (a) — Optimized values of various considered controllers using MOA technique

PID -TID Controller					
$K_{CP1} = 0.8810$	$K_{CI1} = 0.2512$	$K_{CD1} = 0.8790$	$K_{CP2} = 0.9000$	$K_{CI2} = 0.2512$	$K_{CD2} = 0.8790$
$K_{CP3} = 0.9240$	$K_{CI3} = 0.252\ 1$	$K_{CD3} = 0.9170$	$K_{CT1} = 0.6242$	$K_{CI1} = 0.2243$	$K_{CD1} = 0.7704$
$n_{C1} = 4.\ 1045$	$K_{CT2} = 0.6002$	$K_{CI2} = 0.2405$	$K_{CD2} = 0.7460$	$_{C}n_2 = 3.0341$	$K_{CD3} = 0.7640$
$K_{CT3} = 0.5908$	$K_{CI3} = 0.3302$	$n_{C3} = 3.0720$			
TID Controller					
$K_{P1} = 0.8215$	$K_{I1} = 0.3094$	$K_{D1} = 0.7940$	$K_{P2} = 0.8604$	$K_{I2} = 0.2803$	$K_{D2} = 0.7720$
$K_{P3} = 0.8700$	$K_{I3} = 0.2190$	$K_{D3} = 0.5709$			
PID Controller					
$K_{P1} = 0.9024$	$K_{I1v} = 0.2152$	$K_{D2\ v} = 0.8970$	$K_{P2\ v} = 0.3802$	$K_{I3\ v} = 0.7245$	$K_{3D} = 0.3000$

Table 1(b) — Performance comparison with the proposed PID–TID controller against PID and TID controllers

Characteristics		PID-TID	TID	PID
	PO	0.00943	0.00998	0.01180
ΔF_1	PU	0.02032	0.02205	0.02520
	ST	50.0500	56.0300	>100.00
	PO	0.00329	0.00457	0.00758
ΔF_2	PU	0.01408	0.01530	0.01709
	ST	38.3800	43.3200	>100.00
$\Delta Ptie_{12}$	PO	0.00148	0.00158	0.00247
	PU	0.00640	0.00750	0.00808
	ST	41.3600	49.5000	>100.00
	PO	0.00180	0.00230	0.00280
$\Delta Ptie_{23}$	PU	0.00180	0.00340	0.00240
	ST	34.5060	45.060	>100.00

iteration: men and females. Females are attracted to the pheromones released by males, and the position of the males in the search area is completely random. In MOA, a fitness function is employed to assess the quality of solutions, reflecting the extent of their improvement. Females choose compatible partners based on the evaluation, and mating with crossover operation results in novel offspring solutions. To inherit traits from both parents and enhance search space exploration, this progeny goes through mutation. Individuals with greater fitness values are chosen for the following generation after the new solutions have been assessed. Until tht termination condition is met. Thus procedure is repeated multiple times. The overall flow of MOA is illustrated in Fig. 5.

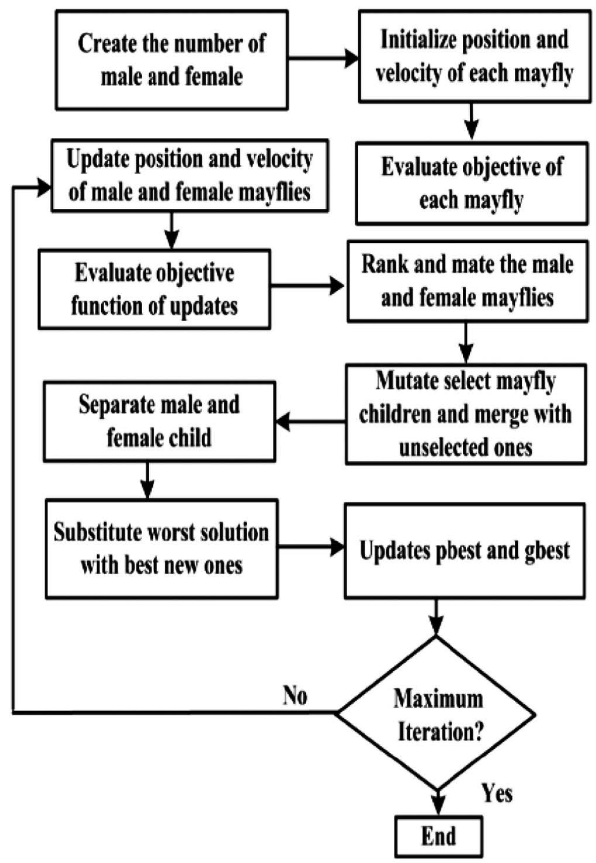

Fig. 5 — Flow chart of MOA

3 Results and Discussion

3.1 System Performance Analysis with Various Controllers

The system with additional controllers, specifically TID, PID, and PID–TID, each assessed separately, is shown in Fig. 1. The controller values are optimized by MOA and its corresponding values are in Table 1 (a). Figure 6 compares and illustrates the dynamic performances of the controllers under consideration, and Table 1 (b) lists the main performance indices like peak undershoot (PU), peak overshoot (PO), and settling time (ST) that were taken from the responses displayed in Fig. 6.

According to a critical evaluation of dynamics in Fig. 6, the performance in Table 1 (b), the suggested PID–TID outperforms in terms of dynamic performance, especially when it comes to ST, PU, and PO. Comparing the PID–TID controller to the other two, the latter shows fewer subsequent oscillations in

Table 2 (a) — Optimized values of proposed PID-TID controller, when system is employed with WTS

K_{CP1} = 0.9234	K_{CI1} = 0.2325	K_{CD1} = 0.8207	K_{CT1} = 0.5100	K_{CI1} = 0.2040	K_{D1} = 0.7941
n_{C1} = 3. 1405	K_{CP2} = 0.8902	K_{CI2} = 0.2650	K_{CD2} = 0.8460	K_{CT2} = 0.5082	K_{I2} = 0.6000
K_{CD2} = 0.8375	n_{C2} = 4.0341	K_{CP3} = 0.9114	K_{CI3} = 0.2360	K_{CD3} = 0. 7963	K_{T3} = 0.4990
K_{CI3} = 0.2550	K_{CD3} = 0. 7963	n_{C3} = 4.0100			

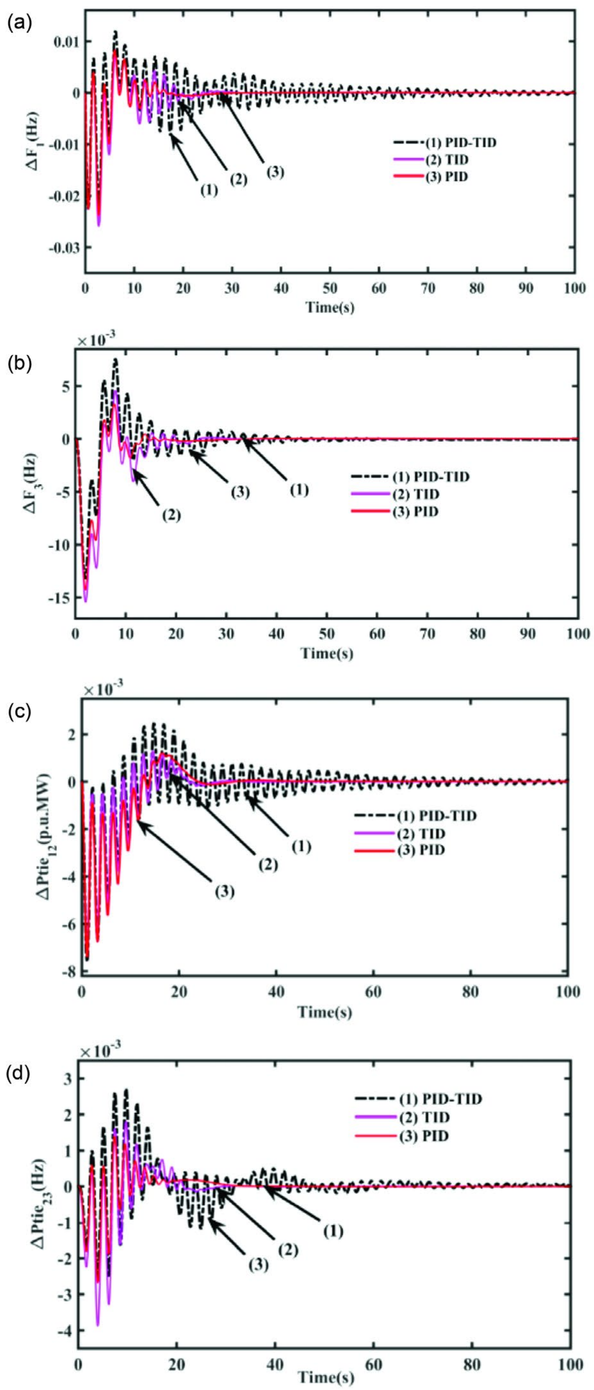

Fig. 6 — Dynamic performance of the system under different controllers (PID-TID, PID, PI,) (a) ΔF_1, (b) ΔF_3, (c) $\Delta Ptie_{12}$, and (d) $\Delta Ptie_{23}$

Table 2 (b) — Key performance indices value comparison with respect to TS only and TS with WTS

Characteristics		With TS and WTS	With only TS
	PO	0.00880	0.00943
ΔF_1	PU	0.01630	0.02032
	ST	37.5000	50.0500
$\Delta Ptie_{12}$	PO	0.00149	0.00159
	PU	0.00746	0.00846
	ST	37.3900	40.4600

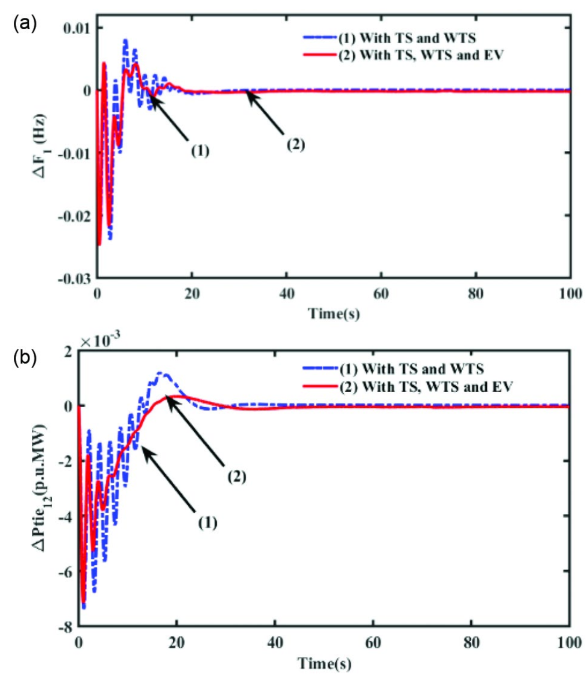

Fig. 7 — System performance with and without WTS unit (a) ΔF_1, and (b) ΔP_{tie12}

the system response. Thus, the cascade PID–TID controller is used in all case studies that follow.

3.2 System Performance Analysis by Employing WTS

The dynamic responses of three-area TS by integrating WTS units across all three areas are analyzed using the PID–TID controller, whose optimal parameters are determined via MOA and are presented in Table 2 (a). A comparative assessment of system performance with and without WTS units is illustrated in Fig. 7. The corresponding key performance indices are summarized in Table 2 (b).

From Fig. 7 and numerical values of Table 2 (b), when the system is provided WTS unit in all the

Table 3 (a) — Optimized values of proposed PID-TID controller, when system is employed with EVs

K_{CP1} = 0.9438	K_{CI1} = 0.2370	K_{CD1} = 0.8200	K_{CP2} = 0.8906	K_{CI2} = 0.2490	K_{CD2} = 0.8362
K_{CP3} = 0.9130	K_{CI3} = 0.2560	K_{CD3} = 0.8640	K_{CT1} = 0.5205	K_{CI1} = 0.2142	K_{CD1} = 0.8000
n_{C1} = 3.4400	K_{CT2} = 0.5202	K_{CI2} = 0.5808	K_{CD2} = 0.8260	n_{C2} = 4.0001	K_{CD3} = 0. 7996
K_{CT3} = 0.5000	K_{CI3} = 0.2404	n_{C3} = 4.2050			

Table 3 (b) — Key performance indices value comparison with respect to TS, WTS and EVs of the system

Responses	Indices	With TS, WTS and EVs	With TS and WTS
	PO	0.00760	0.00880
ΔF_1	PU	0.01290	0.01630
	ST	35.3000	37.5000
	PO	0.00011	0.00149
$\Delta Ptie_{12}$	PU	0.00260	0.00746
	ST	36.0220	37.3900

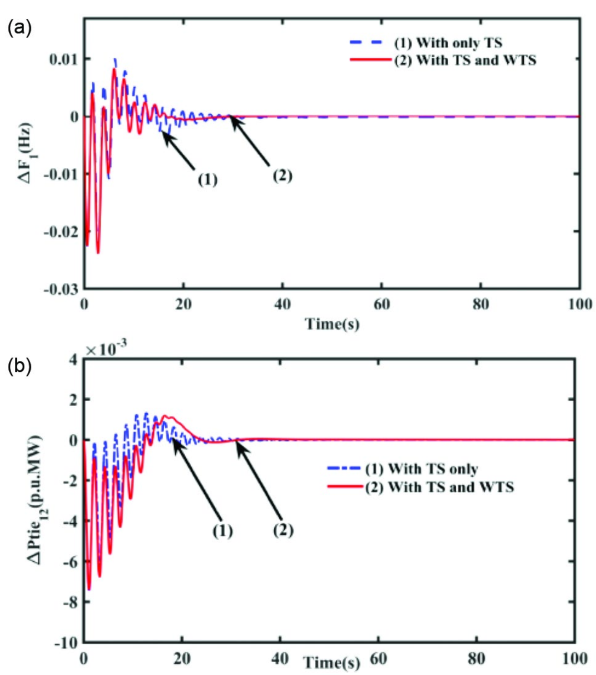

Fig. 8 — System performance with respect to TS integrated WTS and TS, WTS and EV (a) ΔF_1, and (b) ΔP_{tie12}

areas, the ST of the system significantly reduces. Moreover, the PO and PU also found lesser when compared to TS only. As a result, it can be concluded that when WTS is integrated in three area TS, over all dynamic profile of the system is enhanced.

3.3 System Performance Analysis by Employing EVs

The dynamic responses of three-area TS, WTS by incorporating EVs across all interconnected regions are analyzed using the PID–TID controller. Controller parameters have been optimized via MOA, and their optimal settings are detailed in Table 3 (a). Figure 8 compares dynamic profiles with and without EVs. The corresponding key performance indices are compiled in Table 3 (b).

Based on the performance indices in Table 3 (b), it is evident that system with WTS and EVs improve dynamics in terms of number of oscillations. Also, the PO, PU and ST are comparatively lower as compared to system with WTS.

3.4 System Performance Analysis by Employing ESD

Now the system is integrated with RFB as an ESD in all the connected areas. The dynamic responses of the system are analyzed using the PID–TID controller. MOA optimizes the controller values; the results are in Table 4 (a). The dynamic profiles comparing the system with WTS and EV versus the system with WTS, EV, and ESD are depicted in Fig. 9. Table 4 (b) provides a summary of the key performance indicators with respect to WTS, EVs and ESD.

From the obtained dynamic response in Fig. 9 and key performance in Table 4 (b), it is evident that when system is integrated with WTS, EVs and ESD, the systems dynamics improves in terms of number of oscillation, PO, PU and ST compared to system with WTS and EVs.

3.5 Evaluations of Robusness of Proposed Controller

To assess the system robustness, change the loading from the nominal 50 % to alternative values, such as ±25 %. A comparison of the system performance at 25 %, 50 %, and 75 % loading levels is shown in Fig. 10.

The dynamic responses in Fig. 10 demonstrate that the cascaded PID-TID controller performs substantially the same when the system loading deviates by ±25 % from the nominal value. Therefore, it can be said that there is no need to change the controller settings to the nominal setting since the PID-TID controller offers stable performance.

Table 4 (a) — Optimized values of proposed PID-TID controller, when system is employed with ESD

K_{CP1} = 0.9234	K_{CI1} = 0.2325	K_{CD1} = 0.8207	K_{CP2} = 0.8902	K_{CI2} = 0.2650	K_{CD2} = 0.8375
K_{CP3} = 0.9114	K_{CI3} = 0.2550	K_{CD3} = 0.8600	K_{CT1} = 0.5100	K_{CI1} = 0.2040	K_{CD1} = 0.7941
n_{C1} = 3.1405	K_{CT2} = 0.5082	K_{CI2} = 0.6000	K_{CD2} = 0.8460	n_{C2} = 4.0341	K_{CD3} = 0. 7963
K_{CT3} = 0.4990	K_{CI3} = 0.2360	n_{C3} = 4.0100			

Table 4 (b) — Key performance indices value comparison with respect to WTS, EVs and ESD

Responses	Indices	With WTS, EVs and ESD	With WTS and EVs
	PO	0.00290	0.00760
ΔF_1	PU	0.01180	0.01290
	ST	25.3000	35.3000
	PO	0.00010	0.00011
$\Delta Ptie_{12}$	PU	0.00034	0.00260
	ST	33.6000	36.0220

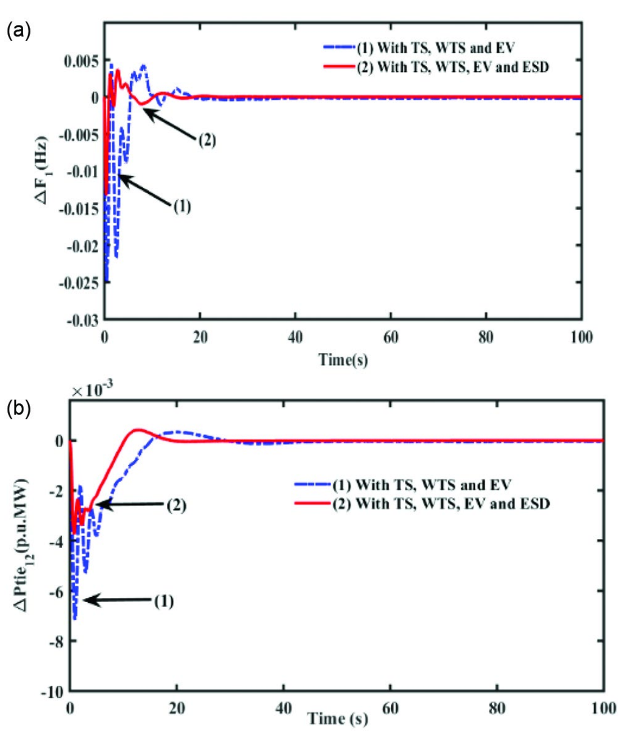

Fig. 9 — Comparison of system performance with respect to TS, WTS, EVS and ESD (a) $\Delta F_{1,}$ and (b) ΔP_{tie12}

4 Conclusion

The effectiveness of PID, TID, and cascaded PID–TID controllers as secondary controllers in a three-area interconnected power system is investigated in this study. Dynamic response analysis reveals that the proposed cascaded PID–TID controller significantly outperforms the conventional standalone PID and TID controllers when the controller parameters are optimally tuned

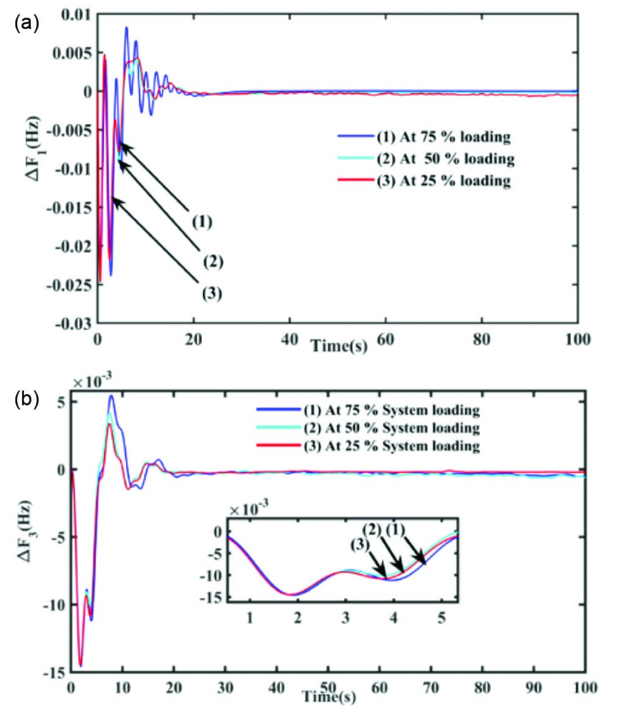

Fig. 10 — System performance at ±25% loading scenario (a) $\Delta F_{1,}$ and (b) ΔP_{tie12}

using the MOA. In addition, the impact of integrating ESDs, EVs, and WTS on overall system dynamics is comprehensively evaluated. The results demonstrate that the coordinated integration of WTS, EVs, and ESD markedly enhances system performance, particularly in terms of reduced peak overshoot, settling time, and peak undershoots. Furthermore, sensitivity analysis confirms that the proposed cascaded controller maintains stable and reliable performance under a wide range of loading conditions without requiring retuning of nominal parameters. These findings highlight the robustness and effectiveness of the proposed control strategy for modern interconnected power systems.

Appendix

1 Thermal System: H_i = 5.00 s, T_{ij} = 0.0860 p.u.MW/rad., T_{gi} = 0.080s, K_{Psi} = 120.0Hz/p.u.MW, F_i = 60Hz,lR_i = 1/2.4 Hz p.u.MW, T_{psi} = 20.0s, T_{CO} = 0.3s, F_{IP} = 0.4, F_{HP} = 0.3, F_{LP} = 0.3, T_{RH} = 4.99, B_i = 0.425MW p.u,

2 WTS: K_{HPi} = 1.25, T_{HPi} = 0.041s, T_{BPi} = 0.6s, K_{Di} = 1.4, K_{PCi} = 0.8

3 Electric Vehicle: KEV = 1, TEV =1, Ri = 2.4 Hz p.u.MW,

4 ESD: Transfer function: $\frac{K_{RFB}}{1+T_{RFB}\,s}$, K_{RFB} =1, T_{RFB} = 0.0001 sec

5 MOA: Max. iteration= 100, damping ratio = 0.8, population size =30, coefficient of learning = 1.0, coefficient of distance = 2.0, coefficient of flight = 1.0, weight of inertia = 0.8, number of offspring = 30, and rate of mutation = 0.01

References

1 Elgerd O I, *Electric energy systems theory: an introduction* (Tata McGraw-Hill, New Delhi), 2nd Edn, 2007, p. 57.

2 Gouran-Orimi S & Ghasemi-Marzbali A, *Appl Soft Comput*, 137 (2023) 110135.

3 Bhagat S K, Babu N R & Chiranjeevi T, *J King Saud Univ Eng Sci*, 37 (2025) 38.

4 Sharma M, Dhundhara S & Sran R S, *Sustain Energy Technol Assess*, 56 (2023) 103025.

5 Debnath M K, Jena T & Mallick R K, *Cogent Eng*, 4 (1) (2017) 1416535.

6 Daraz A, Malik S A, Basit A, Aslam S & Zhang G, *Fractal Fract*, 7 (1) (2023) 89.

7 Tan R, Nguyen H H, Foo E Y S, Yau D K Y, Kalbarczyk Z, Iyer R K & Gooi H B, *IEEE Trans Inform Forensic Secur*, 12 (7) (2017) 1609.

8 Babu N R & Saikia L C, *Eng Sci Technol Int J*, 33 (2022) 101072.

9 Kushwaha P, Prakash V, Yamujala S & Bhakar R, *J Energy Storage*, 62 (2023) 106944.

10 Dekaraja B & Saikia L C, *Energy Storage*, 4 (6) (2022) e370.

11 Bhagat S K, Saikia L C & Babu N R, *Iran J Sci Technol Trans Electr Eng*, 48 (2024) 143.

12 Bhagat S K & Saikia L C, *Electric Power Syst Res*, 222 (2023) 109522.

13 Tasnina W & Saikia L C, *J Renew Sustain Energy*, 10 (2018) 024101.

14 Sharma M, Prakash S, Saxena S & Dhundhara S, *Electric Power Components Syst*, 48 (18) (2020) 1912.

15 Dutta A & Prakash S, *Environ Prog Sustain Energy*, 39 (2020) e13329.

16 Biswas S, Roy P K & Chatterjee K, *IETE J Res*, 69 (3) (2023) 1486.

17 Ahmed M, Magdy G, Khamies M & Kamel S, *Int J Electrical Power & Energy Systems,* 135 (2022) 107528.

18 Babu N R & Saikia L C, *IET Renew Power Generation*, 15 (5) (2021) 1116.

19 Padhy S, Panda S & Mahapatra S, *Eng Sci Technol Int J*, 20 (2) (2017) 427.

20 Babu N R & Saikia L C, *IET Renew Power Generation*, 13 (12) (2019) 2221.

21 Vigya, Shiva C K, Vedik B & Mukherjee V, *Energy Syst*, 14 (2023) 133.

22 Manohar A & Yadav J, *International Conference on Computational Intelligence, Communication Technology and Networking (CICTN), Ghaziabad, India*, 2023, p. 339.

23 Saha A, Dash P, Chiranjeevi T & Babu N R, *J Taibah Univ Sci*, 18 (1) (2024) 2334004.

24 Bhagat S K, Behera S, Saha A, Bal T, Chiranjeevi T, Devarapalli R & Babu N R, *SN Comp Sci*, 4 (2023) 138.

25 Babu N R, Chiranjeevi T, Devarapalli R & Bhagat S K, *J Eng Res*, 11 (2) (2023) 100060.

26 Saha A, Chiranjeevi T, Devarapalli R, Ram Babu N, Dash P & Màrquez F P G, *Archives Control Sci*, 33 (4) (2023) 861.

27 Babu N R, Chiranjeevi T, Saha A & Bhagat S K, *J Eng Res*, 11 (4) (2023) 425.

28 Babu N R, Chiranjeevi T, Devarapalli R, Knypiński Ł & Màrquez F P G, *Archives of Control Sci*, 33 (2) (2023) 371.

29 Zervoudakis K & Tsafarakis S, *Comp Ind Eng*, 145 (2020) 106559.

30 Debbarma S & Dutta A, *IEEE Trans Smart Grid*, 8 (6) (2017) 2554.